Electronic Supplementary Information (ESI)

Engineering of supramolecular photoactive protein architectures: Defined co-assembly of photosystem I and cytochrome *c* using a nanoscaled DNA-matrix

Kai R. Stieger*[a], Dmitri Ciornii[a], Adrian Kölsch[b], Mahdi Hejazi[b], Heiko Lokstein[c], Sven C. Feifel[a], Athina Zouni[b] and Fred Lisdat*[a]

I) MALDI verifcation of PSI:cyt *c* complex formation in solution

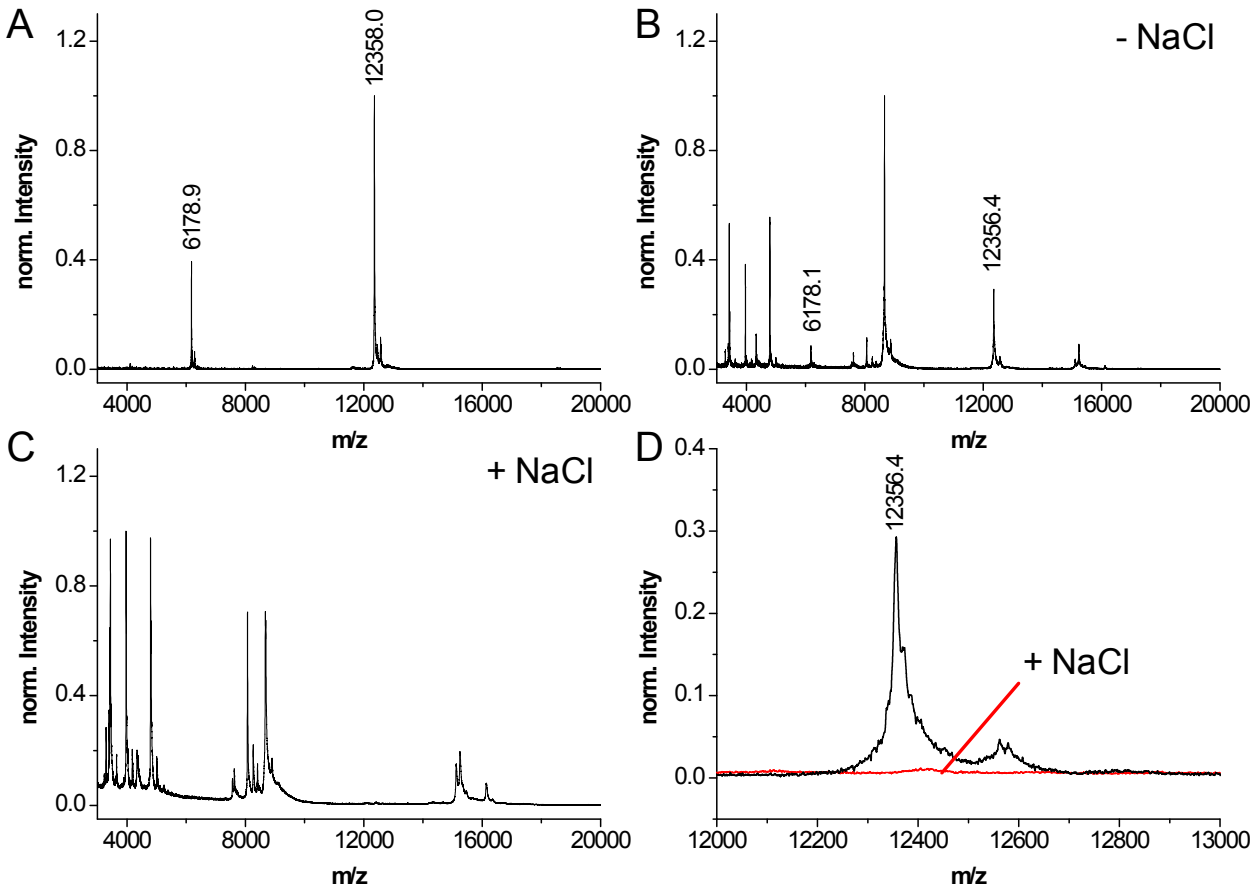

Figure S1. Mass spectrometry analysis of PSI:cyt *c* complexes. **(A)** MALDI-TOF spectrum of cyt *c*. The characteristic peaks at 12,358 and 6,179 corresponds to the molecular mass of cyt *c* (one and two protonated mass, respectively). **(B)** MALDI-TOF spectrum of PSI:cyt *c* complexes formed in solution with a molecular ratio of 1:50 in phosphate buffer (5 mM, pH 7). Cyt *c* can be found in the spectrum with peaks at 12,356 and 6,178. **(C)** MALDI-TOF spectrum of PSI:cyt *c* complex solution after addtion of 100 mM NaCl. Cyt *c* characteristic peaks at 12,358 and 6,179 are missing due to disassembly of the PSI:cyt *c* complexes and removal of free cyt *c* by filtration. **(D)** Comparison between mass spectra of the molecule ion peak of cyt *c*. After addition of 100 mM NaCl to the complex solution and filtration of the PSI:cyt *c* complex solution to remove the free cyt *c* molecules the peak at 12,356 is missing. Spectra have been normalized to the highest peaks.

II) Photocurrent response of different PSI:cyt *c* mixtures

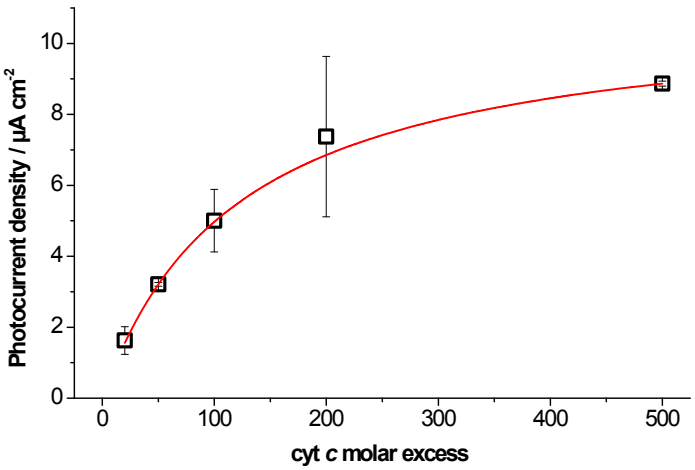

Figure S2. Photocurrent density in dependency of the molar excess of cyt *c* to PSI. Electrodes have been first modified with a cyt *c* ML, then cytc and PSI are co-assembled from protein mixtures with different molar excess of cyt *c* versus PSI. Photochronoamperometric measurements have been carried out under aerobic conditions, phosphate buffer (5 mM, pH 7) at a potential of -100 mV (vs. Ag/AgCl) using white light of 20 mW cm^{-2} (n = 4).

III) Peak separation of Au-ML-DNA-[PSI:cyt *c*/DNA]$_n$ electrodes

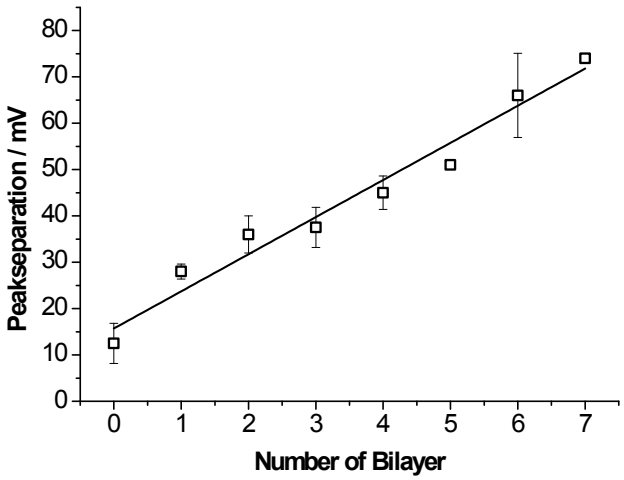

Figure S3. Peak separation of Au-ML-DNA-[PSI:cyt *c*/DNA]$_n$ electrodes in dependence of the number *n* of bilayers. Peak separation increases linearly with the number of bilayers. Measurements have been performed with a scan rate of 100 mV s^{-1} between -300 mV and 300 mV in phosphate buffer (5 mM, pH 7) in the dark. Linear fit was performed with an adjusted R^2 = 0.962.

IV) Photocatalysis of Au-ML-DNA-[PSI:cyt *c*/DNA]$_n$ electrodes

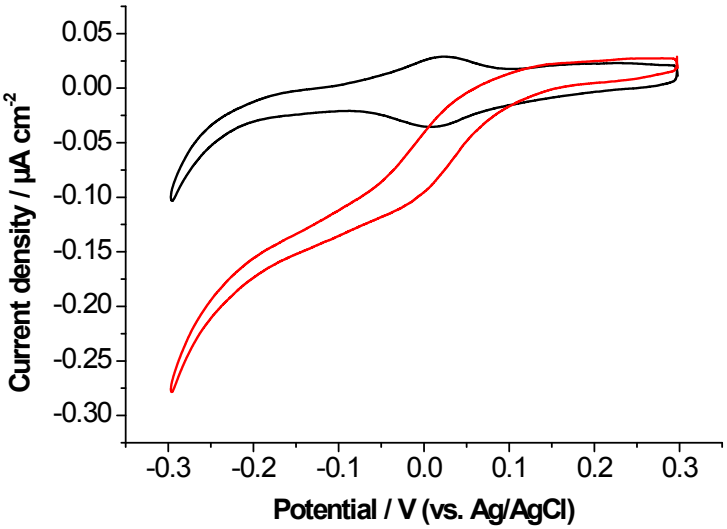

Figure S4. Photo-induced catalytic current of the Au-ML-DNA-[PSI:cyt *c*/DNA]$_n$ electrode. The experiment has been performed in the dark (black) and with 50 mW cm^{-2} of white light (red) at a scan rate of 10 mV s^{-1} in aerobic phosphate buffer (5 mM, pH 7) containing 1 mM MV^{2+}. Cathodic catalysis starts at 80 mV vs. Ag/AgCl.

V) SPR of Au-ML-DNA-[PSI:cyt *c*/DNA]$_n$ assembly

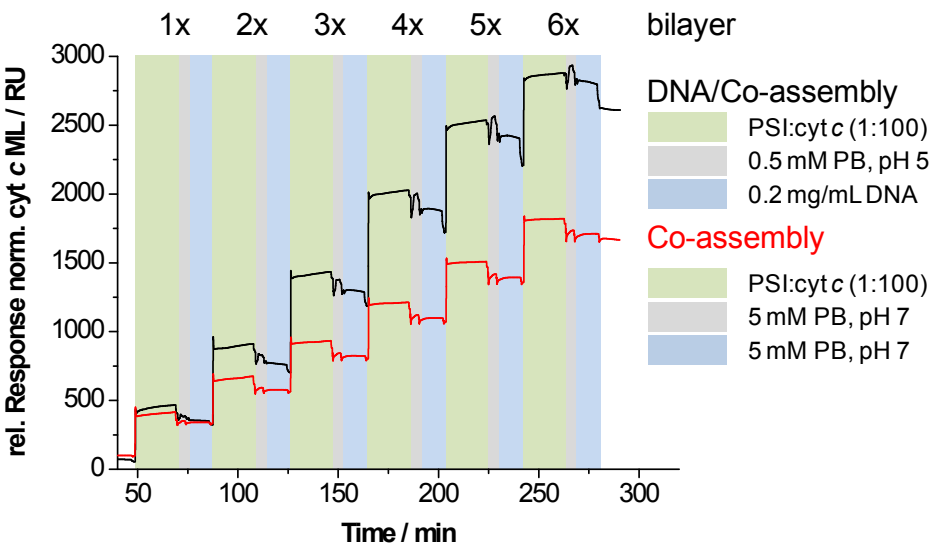

Figure S5. Surface plasmon resonance measurements of the assembly of photosystem I (PSI) and cytochrome *c* (cyt *c*) on a cyt *c* monolayer (cyt *c* ML) with and without the use of DNA (Au-ML-DNA-[PSI:cyt *c*/DNA]$_n$ and Au-ML-[PSI:cyt *c*]$_n$ assembly for n = 1, 2, 3, 4, 5, 6). An intermittent buffer wash with phosphate buffer (PB) between the PSI:cyt *c* and DNA layer has been performed. The sensogram starts after the incubation of a cyt *c* ML (both systems) and one DNA layer (only for the DNA/co-assembly system) and have been normalized to the cyt *c* mass signal of the cyt *c* ML. The rather minor differences for the first bilayer between the control (co-assembly) and the DNA/co-assembly can be explained by a small increase of surface roughness after the first DNA layer incubation, which raises the accessible area for the protein complexes. Here, for all assembly steps (both control and DNA assembly) the same injection time was choosen, which exhibit a different kinetic behaviour compared to Fig. 2 (the experiment has been performed under varying injection times of the PSI:cyt *c* complex solution).

VI) Photocurrent control without cyt *c* in the multilayer assembly: Au-ML-DNA-[PSI/DNA]$_6$

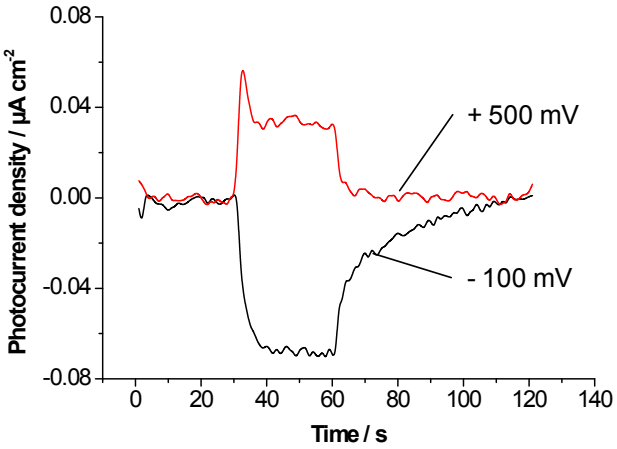

Figure S6. Photocurrent measurements of the Au-ML-DNA-[PSI/DNA]$_6$ electrode. The electrode assembly contains a cyt *c* monolayer (ML) separated by DNA from the PSI/DNA assembly. The photocurrent measurement at two different potentials (-100 mV, +500 mV vs Ag/AgCl) exhibit only minor photocurrent densities and cathodic and anodic photocurrents are observed. This experiment shows, that cyt *c* is nescessary for the high unidirectional photocurrent generation of a multilayer assembly – DNA does not contribute to the electron transfer. The experiments have been performed at RT in phosphate buffer (5 mM, pH 7) using white light (20 mW cm^{-2}, 30 s pulse) at a potential of -100 mV (black) and +500 mV (red) vs. Ag/AgCl.

VII) Long term storage experiments of the Au-ML-DNA-[PSI:cyt *c*/DNA]$_6$ electrode

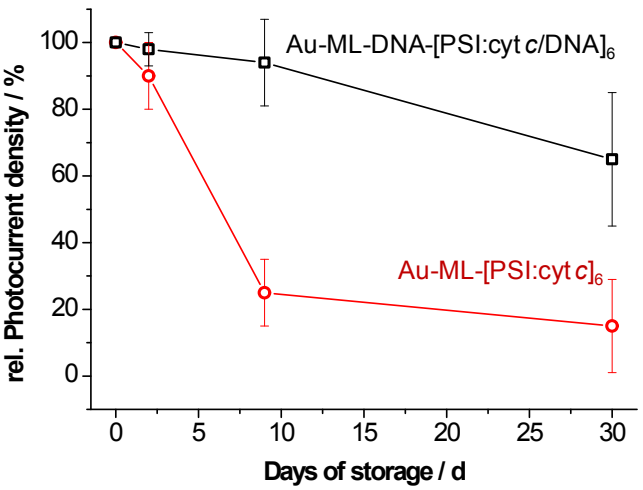

Figure S7. Relative photocurrent density of the Au-ML-DNA-[PSI:cyt *c*/DNA]$_6$ (black) and Au-ML-[PSI:cyt *c*]$_6$ electrode vs. storage time. The experiment shows the measurement of each type of electrodes after a certain time of storage (dry at 4 °C in the dark). The electrodes have been measured first after preparation, than subsequently after 2, 9 and 30 days of storage. The experiments have been performed at RT in phosphate buffer (5 mM, pH 7) using white light (20 mW cm^{-2}) at a potential of -100 mV vs. Ag/AgCl.

VIII) Light source spectrum (white light)

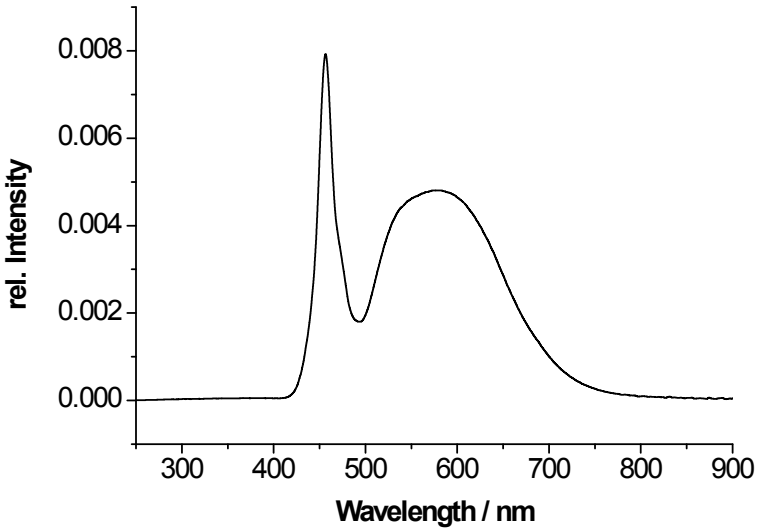

Figure S8. Spectrum of the white light source used in all experiments. The spectrum was normalized to an integral area of 1. Characteristic peak values are at 456 nm and 576 nm.

IX) Interaction between cyt *c* and PSI in solution

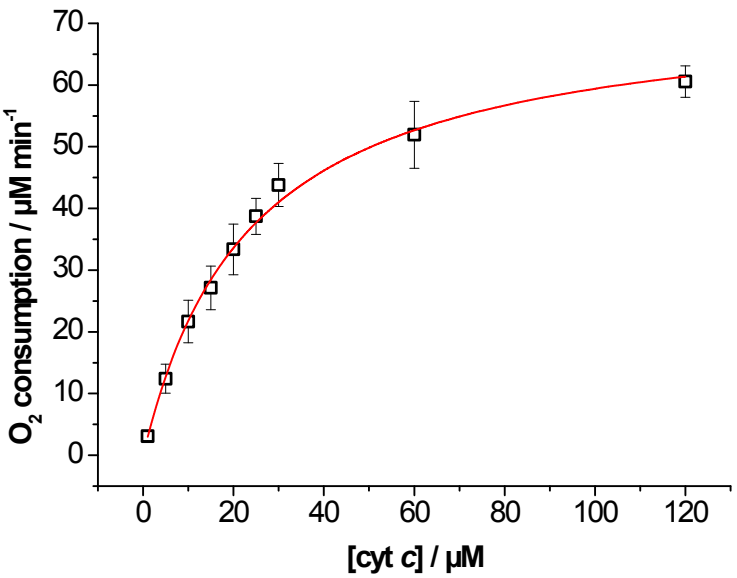

Figure S9. O_2 consumption of PSI vs. cyt *c* concentration in solution. The experiment has been performed at 20 °C under aerobic conditions and saturating light (700 µmol m^{-2} s^{-1}) in phosphate buffer (5 mM, pH 7) containing 170 µM MV^{2+}, 0.05 % ß-DM, 1 mM Na-ascorbate, 20 nM PSI and a variable concentration of cyt *c*. Data have been fitted with a Michaelis-Menten equation with a K_M value of 23 ± 3 µM and a v_{max} value of 74 ± 2 µM min^{-1}. For the interaction of PSI with cyt *c* a catalytic rate of 20 ± 1 s^{-1} can be calculated. The experiment shows, that cyt *c* enhances the oxygen consumption of PSI dramatically, as it provides the electrons for the photoexcited P700 reduction.

X) Photoaction spectra of the Au-ML-DNA-[PSI:cyt *c*/DNA]$_6$ electrode

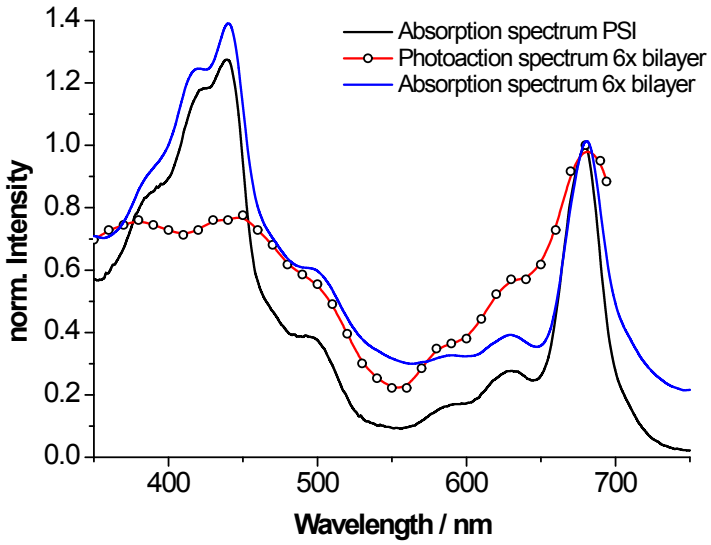

Figure S10. Photoaction spectrum of an Au-ML-DNA-[PSI:cyt *c*/DNA]$_6$ electrode in comparison to the absorption spectrum of PSI in phosphate buffer (5 mM, pH 7) and with the absorption spectrum of a glass-APTES-DNA-[PSI:cyt *c*/DNA]$_6$ surface, all normalized at the peak at 680 nm. The spectra verify the origin of the photocurrent, since the photoaction spectrum follows the general lineshape of absorption spectra of PSI in solution and in the assembly. Additionally, comparison between the absorption spectra of PSI in solution and the one on the glass-APTES-DNA-[PSI:cyt *c*/DNA]$_6$ surface reveals a similar wavelength dependence. However, due to incorporation of cyt *c* and DNA into the assembly the surface spectrum has an increased background. Photoaction spectra have been obtained with monochromatic light (bandwidth 15 nm, intensities > 10 mW cm^{-2}) in aerobic phosphate buffer (5 mM, pH 7). The broadening of the peaks is due the relatively high bandwidth of the monochromatic light. The lower photocurrent generation in the region of 400 to 450 nm is possibly due to competing absorption of the cyt *c* Soret band. Spectra are the averages of 3 independent measurements.

XI) Proposed electron transfer mechanism for the Au-ML-DNA-[PSI:cyt *c*/DNA]$_n$ electrode

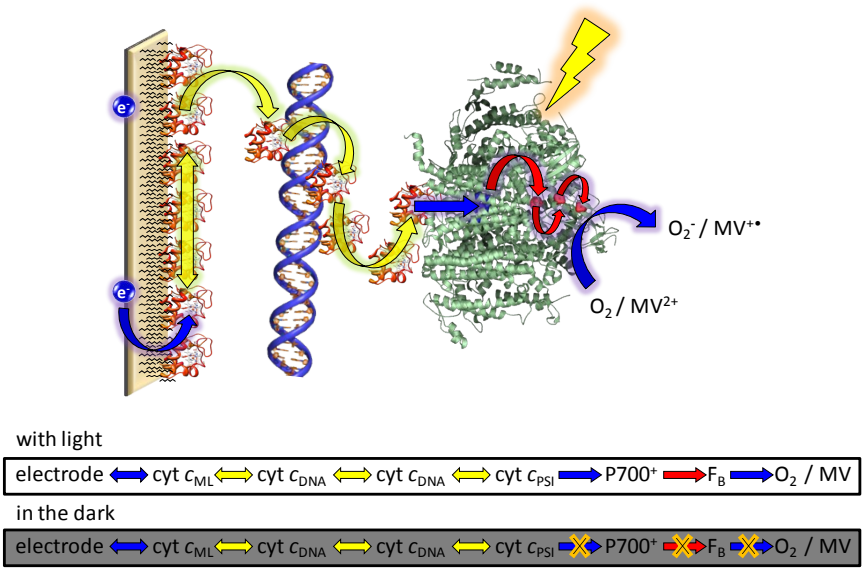

Figure S11. Schematic representation of the proposed cathodic electron transfer mechanism for the Au-ML-DNA-[PSI:cyt *c*/DNA]$_n$ electrode. Electrons are injected into the cyt *c* monolayer (cyt c_{ML}) and relayed via cyt *c* – cyt *c* self exchange. Cyt *c* molecules bound to DNA molecules in proximity can exchange electrons. Finally, electrons are transferred to PSI-bound cyt *c* and reduce photoexcited $P700^+$. Within PSI complex, electrons flow to the terminal iron-sulfur cluster F_B which is oxidized by oxygen or methyl viologen. Heterogenous electron transfer processes are indicated with blue, homogenous with yellow, and intramolecular ones with red arrows.

Electronic Supplementary Information (ESI)